Nanoscale Thermomechanics of Wear-Resilient Polymeric Bilayer Systems

Tassilo Kaule,[†] Yi Zhang,[†] Sebastian Emmerling,[†] Sascha Pihan,[†] Renate Foerch,[†] Jochen Gutmann,[†,§] Hans-Jürgen Butt,[†] Rüdiger Berger,[†,*] Urs Duerig,[‡] and Armin W. Knoll[‡,*]

[†]Max Planck Institute for Polymer Research, Ackermannweg 10, 55128 Mainz, Germany and [‡]IBM Research—Zurich, Säumerstrasse 4, 8803 Rüschlikon, Switzerland. [§]Current address: Department of Chemistry and Center for Nanointegration Duisburg-Essen (CeNIDE), University Duisburg-Essen, Universitätsstr. 5, D-45117 Essen, Germany.

ABSTRACT We explore the effect of an ultrathin elastic coating to optimize the mechanical stability of an underlying polymer film for nanoscale applications. The coating consists of a several nanometer thin plasma-polymerized norbornene layer. Scanning probes are used to characterize the system in terms of shear-force-induced wear and thermally assisted indentation. The layer transforms a weakly performing polystyrene film into a highly wear-resistive system, ideal for high-density and low-power data storage applications. The result can be understood from the indentation characteristics with a hot and sharp indenter tip. The latter gives rise to a deformation mode in the fully plastic regime, enabling a simple interpretation of the results. The softening transition and the yield stress of the system on a microsecond time scale and a nanometer size scale were obtained. We show that the plastic deformation is governed by yielding in the polystyrene sublayer, which renders the overall system soft for plastic deformation. The ultrathin protection layer contributes as an elastic skin, which shields part of the temperature and pressure and enables the high wear resistance against lateral forces. Moreover, the method of probing polymers at microsecond and nanometer size scales opens up new opportunities for studying polymer physics in a largely unexplored regime. Thus, we find softening temperatures of more than 100 °C above the polystyrene glass transition, which implies that for the short interaction time scales the glassy state of the polymer is preserved up to this temperature.

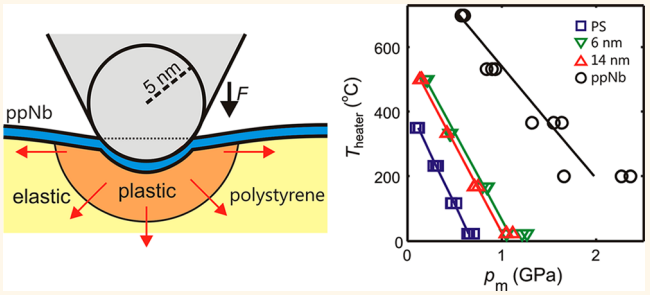

KEYWORDS: protective coating · plasma polymerization · thin polymer films · data storage · indentation · time–temperature superposition · scanning force microscopy

The work reported here was motivated by development needs of a polymer medium for thermomechanical data storage.[1] The technology relies on the reversible writing of information by means of hot embossing using a heated tip to create nanometer scale patterns which represent the data. The requirements on the polymer medium can be phrased in terms of two conflicting properties which need to be reconciled: (1) high surface wear resistance and (2) high plasticity. Careful tuning of the cross-linking between the polymer chains in terms of topology and density was one strategy explored to achieve this goal.[2] As an alternative, one may conceive a bilayer system consisting of a tough surface coating providing wear resistance and a soft polymeric underlayer providing the plasticity functionality.

The concept of polymeric thin film coatings is a widely used strategy to improve materials properties, for example, in the form of antireflective,[3] anticorrosive,[4] water-repellent,[5] and wear-protective[6−8] layers. For our application, the critical issue is the fact that the surface layer needs to be very thin, typically not more than 10 nm. This ensures that heat and mechanical stress stimuli applied to the surface of the coating layer are efficiently transferred into the soft polymeric underlayer which in turn responds by a plastic deformation. The method of choice to obtain such thin coatings is plasma polymerization.[9] Highly cross-linked and thus mechanically stable layers are obtained with excellent control of the film thickness and strong adhesion to the underlying bulk polymer. For the studies reported here, we used polystyrene (PS) as soft underlayer and a surface coating deposited from a norbonene precursor gas in the plasma reactor.

Writing of the data patterns is closely related to nanoindentation, which has been used for quantitative measurements of mechanical material parameters such as elastic

* Address correspondence to ark@zurich.ibm.com, berger@mpip-mainz.mpg.de.

Received for review October 30, 2012 and accepted December 11, 2012.

Published online December 21, 2012
10.1021/nn305047m

modulus and yield strength in the past.[10] By imaging cold written indents, the elastic modulus, hardness, and plasticity index have been derived from measured force depth curves on sputter-deposited organic films.[11] Nanoindentation has been complemented by microthermal analysis providing additional information on thermal material properties.[12,13] Recently, hot scanning probe tips were used to study the softening of polymers at the glass transition[14] on a length scale of nanometers and a time scale of seconds. Driven by our application, we further expand the method by studying the indentation characteristics on a microsecond time scale using hot indenter tips with an apex radius of less than 10 nm. This allows us to explore time–temperature correlations in a temporal and spatial regime, which is rarely addressed experimentally, and to study polymer dynamics in a transitional non-equilibrium state. Furthermore, we can study the yield dynamics at high strain rates on the order of 10^5 s^{-1} in a temperature range from room temperature to the softening temperature of the system.

The paper is organized in two parts. First, we discuss the fabrication and the wear characteristics of the bilayer samples and the performance of the overall system from a data storage perspective. In particular, we show that the bilayer system is wear-resistant and exhibits the same shape-memory effect as has been observed in cross-linked polymers, and we demonstrate high-density writing of patterns corresponding to a data density of 1.8 Tb/in^2. In the second part, the thermomechanical behavior of the system at microsecond time scales is studied in detail by analyzing the indents as a function of force and tip temperature. We show that the surface coating acts like an elastic membrane, and plastic yielding occurs in the PS underlayer. However, the surface coating gives rise to a rescaling of the temperature and stress in the underlayer which manifests itself as shifts of the yield stress, Y, and the softening temperature, T_s, toward higher values with respect to the uncoated PS sample. We also find a linear dependence of Y on temperature. Most remarkably, the measured softening temperature is approximately 100 °C higher than expected from the bulk value of the glass transition temperature, and the measured shift can be rationalized in terms of glass dynamics with an activation energy of 49 kcal/mol as expected for PS.

RESULTS AND DISCUSSION

The bilayer samples studied in this paper consisted of 100 nm thick polystyrene (PS) films spin coated on a Si wafer. The protective coatings were deposited on the PS films by means of plasma polymerization of norbornene (ppNb). By adjusting the deposition conditions, samples with a ppNb layer thickness ranging from 6.5 to 25 nm were fabricated (see Methods section for details). Plasma polymerization is known to form uniform and homogeneous protection layers with low surface roughness.[6] Here, the root-mean-square roughness was <1 nm per μm^2 for all films. The layers were stable, showing no signs of dewetting, delamination, or cracking. The latter indicates that the ppNb layer is mechanically tough. The measured water contact angle of 80 to 90° on the ppNb layer shows that the surface is hydrophobic.

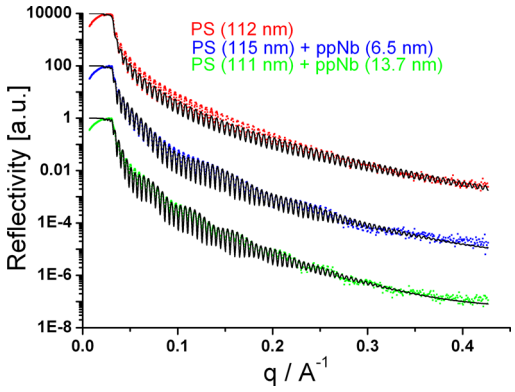

Figure 1. XRR data of a pristine spin-coated PS film and two PS films covered with ppNb protection layers with different thicknesses. For better visibility, the normalized data of the pristine PS film and the 6.5 nm ppNb protected film are multiplied by 10 000 and 100, respectively. The black lines represent fits based on Parrat's formalism.

Thin Film Characterization. X-ray reflectivity (XRR) measurements were used for determining the thickness of the layers in the sample stack. The XRR analysis of ppNb-covered PS samples revealed two characteristic oscillations (Kiessig fringes) in reflectivity of (i) the spin-coated PS layer and (ii) the ppNb cover layer (Figure 1). The beating pattern corresponds to the thinner ppNb and the interference fringes to the thickness of the PS layer. The exact thickness of both layers was determined using a model based on Parrat's formalism.[15] On the basis of this model, we obtained ppNb layer thicknesses of 6.5 and 13.7 nm with a standard error of ±0.1 nm, respectively. The PS film thickness corresponded to 115 and 111 nm, respectively. The two ppNb-protected samples were compared to a blank PS sample and a "bulk" ppNb sample (≈250 nm thick ppNb layer on PS) for reference.

We verified the wear protection function of the ppNb coating by scanning force microscopy (SFM). A nanowear test consisted of 100 scans of the same area in contact mode at a tip load of 10 nN.[16] For the bare PS film, a significant increase in rms roughness from 0.6 to 2.78 nm before and after the wear test was observed, which is consistent with published results (Figure 2A).[17] In contrast, no measurable increase of the roughness was detected on the ppNb-protected samples, demonstrating the anticipated wear resistance (Figure 2B). In fact, the coated samples exhibit wear resistance properties similar to those of highly cross-linked polymer films.[2]

Reversible Thermomechanical Indentation. The ppNb-PS samples were tested for their nanoindentation properties

in the context of thermomechanical data storage applications. The results shown here were obtained using samples with the thinnest, viz. 6.5 nm, ppNb protective layer, which are expected to yield the lowest indentation force. Thermomechanical data writing (see Methods section for details) was performed at a tip heater temperature of 350 °C, a normal force of 80 nN (Figure 3A,C), and using a force and heater pulse duration of 10 μs. A logical one state was encoded as an indentation, a zero as no indentation. The data field consisted of 48 lines of bits (tracks) with 200 bits in each track. The bits along the track were separated by 13.4 nm, which was half the intertrack distance, 26.8 nm, corresponding to an information areal density of $(25.4\ \text{mm})^2/(26.8\ \text{nm} \times 13.4\ \text{nm}) = 1.8\ \text{Tb/in}^2$. The preamble at the beginning of each track (from left to right) consists of 10 repetitions of the logic [1 0] sequence, yielding clearly separated individual indents spaced by 26.8 nm representing the [1]'s (see Figure 3C). After the preamble, random data were written. Note that the indents of adjacent ones merged to form elongated continuous grooves. The average depth of the written features was 3 ± 1 nm, which is sufficient for low error rate detection of the data.[18]

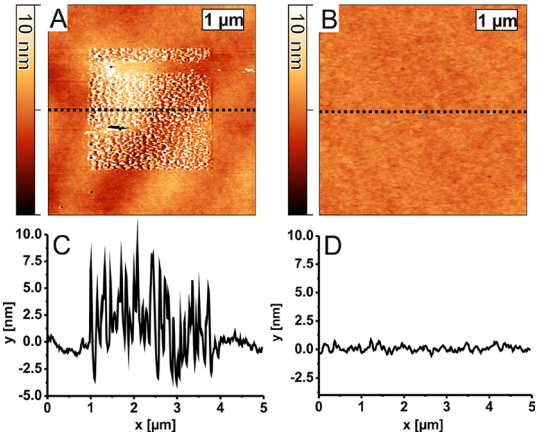

Figure 2. Nanowear test experiment: A 3 × 3 μm^2 area was scanned in contact mode 100 times at a normal force of 10 nN. (A) Result on a pristine PS film having a thickness of 113 nm. Ripples are formed due to the low wear resistance of PS. (B) Same test on a PS film protected with a 6.5 nm thick ppNb layer shows no sign of wear. (C,D) Cross sectional profiles along the dotted lines in panels A and B, respectively.

Previous studies on cross-linked polymer media have revealed that closely spaced indents interact *via* tensile stress components in an annular ring around a written indent, leading to the partial erasure of nearby indents.[19] When this interaction is exploited, an indented surface can be brought back to a flat state by overwriting it with densely spaced indents. The erase demonstration was performed on a larger field overlapping the original written field by a margin of ≈100 nm on each side using the same temperature, force, and pulse duration parameters as for the initial writing of the data pattern. With reference to Figure 3B, the field was scanned from left to right and from the bottom to the top. In each track, a series of logic [1]'s was written at a pitch of 13.4 nm and using the same pitch for the track spacing (doubling the number of written lines). Qualitatively, one may rationalize the erase operation in the following way: Writing of the first erase track results in a continuous linear groove. Since nanoindentation is volume preserving (we neglect bulk compression), the indented volume is pushed to the side, resulting in a

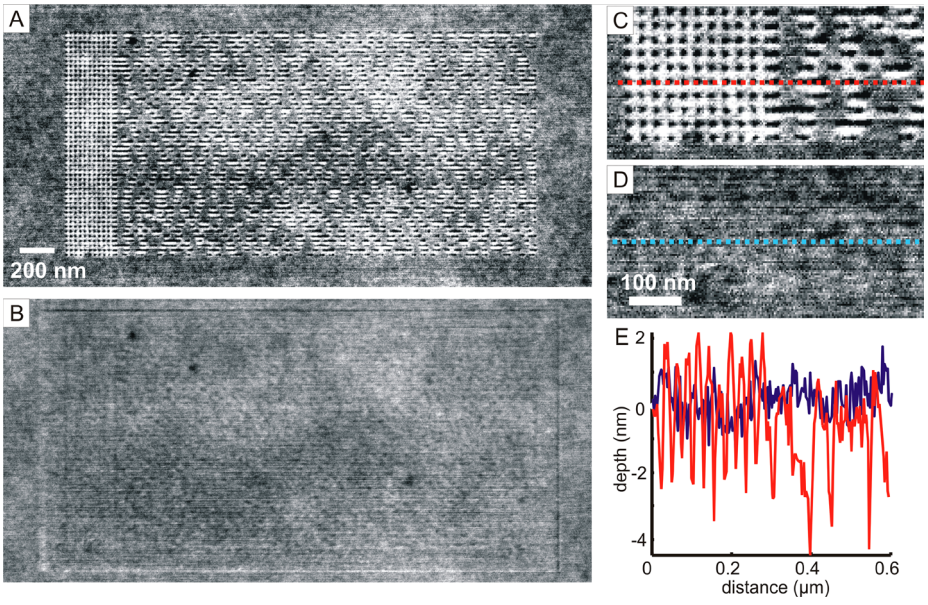

Figure 3. Thermomechanical writing and erasing of bit patterns. (A,C) Bit field written in the layered media with the thinnest ppNb layer of 6.5 nm. (B,D) Same areas as, respectively, displayed in panels A and C after performing an erase operation. (E) Cross sectional profiles along a line of grooves (red line) and at the same position after erasing the data (blue line), corresponding to the dotted lines in panels C and D, respectively. The depth of the grooves is between 2 and 4 nm. The erased surface has a roughness of ≈2 nm peak to peak, similar to the roughness of a virgin surface.

pile-up rim along the written groove. A reminiscent of the rim is clearly visible as a bright line at the bottom of the erased field. The second written track overlaps with the rim of the first track. The rim is pushed back into the first groove, approximately half filling it, and the other half of the groove volume is provided by the rim of the newly written track. By repeating the process, a groove is propagated from the bottom to the top which irons out the previously thermomechanically embossed surface relief. Note that erasing is incomplete for the last written groove, which is visible at the top of the field, and also at the beginning and the end of a track line, showing up as an elevated rim and depression, respectively.

The perfection of erasing can be seen from a direct comparison of the surface topography before (Figure 3C) and after erasing (Figure 3D). A line cross section along a data track (Figure 3E) shows that all singular indents as well as grooves have been completely flattened out. Most remarkably, one also sees that the long wavelength roughness is not altered by the erase operation. In quantitative terms, the root-mean-square roughness normalized to an area of 1 μm^2 after erasing was 0.55 nm_{rms}, similar to the roughness of 0.50 nm_{rms} of the virgin surface.

Writing and erasing of the bit field were done at 350 °C tip heater temperature and 80 nN applied normal force. To achieve a similar quality of writing in highly cross-linked recording media, such as highly cross-linked polyaryletherketones,[2] much higher temperatures of typically 500 °C had to be applied at tip forces below 100 nN. A high degree of cross-linking was necessary to achieve sufficient surface wear resistance and for enabling thermomechanical erasing. On the other hand, cross-linking leads to a substantial increase of the softening temperature in the polymer which is reflected in high values of the writing temperature. All of these important issues can be elegantly solved with the bilayer concept. Being able to use uncross-linked polymers with correspondingly low values of the softening temperature decreases the risk of thermal decomposition of the material and excessive wear of the tips. In addition, the highly cross-linked and hydrophobic nature of the protection layer reduces the chance of creating and picking up unwanted fragments, which would impair the read and write performance. For all experiments shown here, tip contamination was not observed on the protected samples. Thus the ppNb-protected PS film exhibits excellent performance for data storage applications.

Quantifying Nanoscale Thermomechanical Properties at Short Interaction Times. The data recording experiments demonstrate that "soft" indentation properties (*i.e.*, low tip temperatures and low applied forces) of the ppNb-PS-layered media can be achieved. In addition, the successful erasing mechanism indicates that the fundamental indentation mechanics is in essence the same as for an uncoated but cross-linked polymer film. These results suggest that indents are frozen in a metastable state stabilized by the elastic coating and that the yielding occurs in the soft PS underlayer.

In the following set of experiments, we quantify the effect of the coatings on the thermomechanical properties of the bilayer system. The experiment consisted of writing an array of indents by varying applied forces (F_{app}) and temperatures of the tip heater (T_{heater}). After writing, the topography of the written indents was recorded. The indents were grouped in a pattern consisting of 32 lines comprising 200 indents in each line. The indent and line spacing was 40 nm in order to minimize interference. The 32 lines were divided into four blocks of 8 lines. Each 8-line block corresponded to a fixed writing temperature, which varied in equally spaced increments between room temperature, the lowest value, and an upper value of 350 °C (for the softest PS sample) to 700 °C (for the hardest bulk ppNb sample). A subset of the blocks written with the respective highest temperature for each sample is depicted in Figure 4A–D. The blocks themselves were divided into four subgroups of two lines containing indents written at constant writing force. The force was adjusted for each writing temperature to yield no visible indents for the lowest force of ≈10 nN and indents with a remnant depth d_{rem} of ≈5 nm for the highest force of up to 450 nN.

The indentation force *versus* remnant indent depth is plotted for several writing temperatures in Figure 4E for the bare PS sample. For lower temperatures and for deeper indents, a higher force is required. Another representation of the same data depicting the force and temperature values required to achieve a certain indent depth is shown in Figure 4F. F_{app} and T_{heater} parameter pairs were obtained by linear interpolation of the depth data at indent depths of d_{rem} = 2, 3, 4, and 5 nm. Similar plots have been measured for all other samples (not shown). For all samples, we observed that the isolines can be fitted with high quality to straight lines (dashed lines in Figure 4F). The lines intersect in a single point on the temperature axis at ($T_s \approx 415$ °C for PS) and approximately zero force. We identify this point with the softening transition of the sample at which it loses its resistance to plastic deformation. Hence this point corresponds to a point of vanishing yield strength.

The temperature values given in Figure 4 are the values of the silicon heater. The heater temperature T_{heater} can be readily measured and calibrated; however, it does not represent the polymer temperature T_{pol} at the tip–sample interface because of the thermal resistance of the nanoscale tip and tip polymer interface. To estimate the temperature at the polymer interface in contact with the hot tip, we use the results of previous simulations.[20] The rise in temperature at the interface is approximately half the temperature

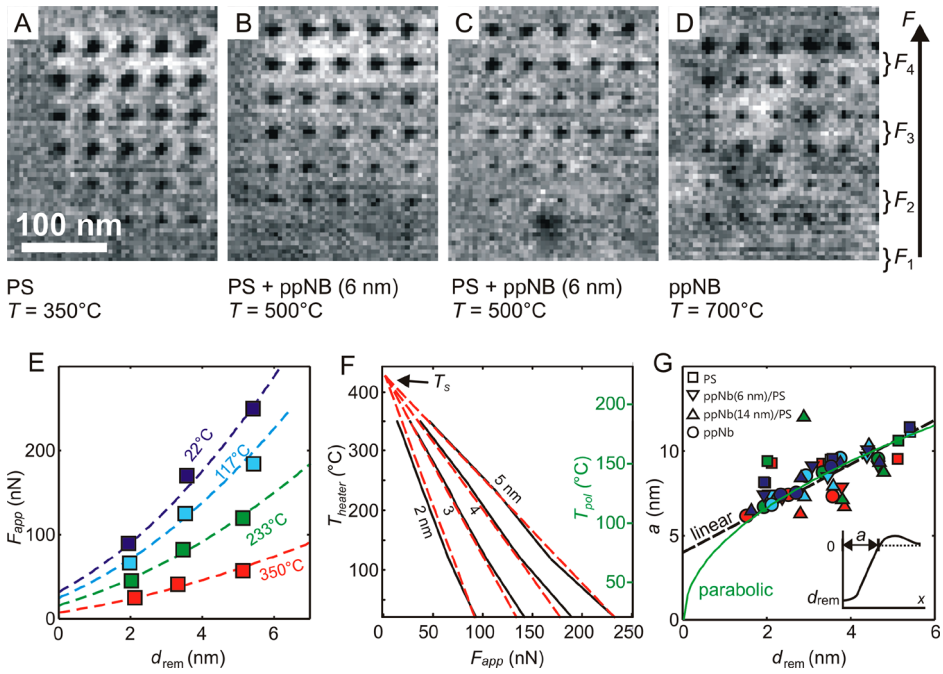

Figure 4. Thermomechanical indent formation. (A−D) Topographies of indent patterns written on (A) PS, (B) 6 nm ppNb on PS, (C) 14 nm ppNb on PS, and (D) bulk-like ppNb (250 nm ppNb on PS). Only data for the hottest tip temperatures are shown. The force increases from bottom to top. (E) Scatter plot and (F) contour plot of the average indent depth as a function of applied force and tip heater temperature. The dashed lines represent the results of a global fit of our model to the data. In F, the extrapolated intersection of the lines is identified with the softening transition T_s of the polymer. (G) Inner radius a of the indents (see sketch in the inset) for all measured indents as a function of indent depth (temperature color code as in panel E). The dashed lines represent fits of a linear and parabolic equation to the data.

difference of the heater to the environment, that is, room temperature T_{RT} (right scale in Figure 4F). In other words, the thermal resistance of tip and interface is of similar magnitude as the thermal spreading resistance in the polymer.[21]

$$T_{pol} = (T_{heater} - T_{RT})/2 + T_{RT} \quad (1)$$

We obtain a value for the softening transition in the PS sample of $T_s = 25\ °C + (415\ °C - 25\ °C)/2 \approx 220\ °C$. At the time scales of seconds of typical material testing experiments, the softening transition would correspond to the glass transition of PS of $T_g \approx 100\ °C$. However, in our experiment, the duration of the heat and force stimuli is applied on a microsecond time scale. Thus for the short time scales, the softening temperature is shifted to significantly higher values.

The linear relation of the writing force with temperature is reminiscent of the previously observed linear scaling of the yield stress with temperature.[22−24]

$$Y = Y_{RT}\left(\frac{T_s - T_{pol}}{T_s - T_{RT}}\right) \quad (2)$$

where T_s denotes the softening temperature defined by zero resistance to plastic deformations ($Y = 0$) and Y_{RT} is the yield stress at room temperature T_{RT}. We note that, at the glass transition temperature T_g, a sharp transition from a finite to a vanishing yield stress has been measured,[22] a feature which we cannot observe in our data.

In order to establish a connection to the geometrical parameters of the indents, the mean indent shape was evaluated using cross-correlation averaging of the indents written under identical conditions (Figure 4A−D, F_1−F_4). The radial profile as sketched in the inset in Figure 4G was determined by an azimuthal averaging procedure assuming a centro-symmetric indent shape. The radial profile is characterized by a remnant indent depth $-d_{rem}$ and an inner indent radius a. The latter is defined by the first intersection of the background zero line with the profile which rises sharply from the negative indent depth $-d_{rem}$ to positive values due to the existence of a rim surrounding the indent.[19]

A plot of the inner radius *versus* the indent depth reveals a linear behavior for all samples under study including the layered samples (Figure 4G). Within the accuracy of the experimental data, all samples showed the same behavior independent of the writing temperature. We find that the inner radius can be described by a linear function of the indent depth d_{rem}:

$$a = a_0 + c d_{rem} \quad (3)$$

where a_0 and c are phenomenological geometrical factors, corresponding to a finite size of the indent in the limit of zero depth and the increase in indent radius with depth, respectively. The geometrical factors used for the fit (black dashed line in Figure 4G) are $a_0 = 4$ nm and $c = 1.3$. For highly cross-linked polystyrene systems, the same linear relation[25] with values of $a_0 > 10$ nm

and $c > 2.6$ was observed. Thus much deeper indents could be written at the same lateral scale for the layered samples studied here.

We note that the observed $a(d_{rem})$ data are also compatible with other models. For example, a possible alternative description would be given by assuming negligible elastic recovery and a parabolic tip of radius R = 11 nm.[26] The curve is shown as green line in Figure 4G according to the parabolic profile $d_{rem} = a^2/2R$. The curve fits the data equally well. However, the underlying assumption of negligible elastic recovery is unphysical as discussed below.

Using the obtained $a(d)$ behavior, we can now calculate the mean pressure p_m below the tip:[27]

$$p_m = \frac{F}{(a(d_{rem}))^2 \pi} \quad (4)$$

Plotting p_m for all indents as a function of heater temperature T_{heater} (Figure 5A), we find that the data points for the respective samples collapse onto linear master curves. We can rationalize this behavior by proposing that the yield stress is proportional to the mean applied pressure p_m

$$p_m = CY \quad (5)$$

with C being a constant. Equation 5 is valid in the framework of fully plastic indentation as discussed below. Combining eqs 2, 4, and 5 yields

$$p_m = \frac{F}{\pi a(d_{rem})^2} = CY_{RT}\left(\frac{T_s - T_{pol}}{T_s - T_{RT}}\right) \quad (6)$$

Equation 6 can be solved for d_{rem} and has been used to obtain the global fits shown in Figure 4. We note that the data are consistent with a finite yield stress at zero permanent deformation (Figure 4E).

Equation 6 also describes the universal linear relation between the p_m and T_{pol}, which is independent of other parameters. This prediction is confirmed by the measured data as shown in Figure 5A for all samples investigated. The intersection of the master curve with the p_m axis yields CY_{RT}. The intersection with the T_{pol} axis yields the softening temperature, T_s, of the sample material (Figure 5B). Note that CY_{RT} is not influenced by the calibration factor used for converting the heater temperature into the polymer temperature. The uncertainty of the calibration factor only adds a proportional systematic error to the temperature axis.

Indentation State. Equation 5 is known to hold in the so-called fully plastic indentation regime. Figure 6 schematically depicts the various indentation states on an inelastic half-space.[26] An indentation is elastic until the yield stress is reached in a small volume of the material which causes first yield (Figure 6A). Up to this point, the stresses can be estimated with high accuracy using elastic indentation models. Applying higher loads, the stress increases and causes the volume exceeding the yield stress to expand (Figure 6B). This regime is called the

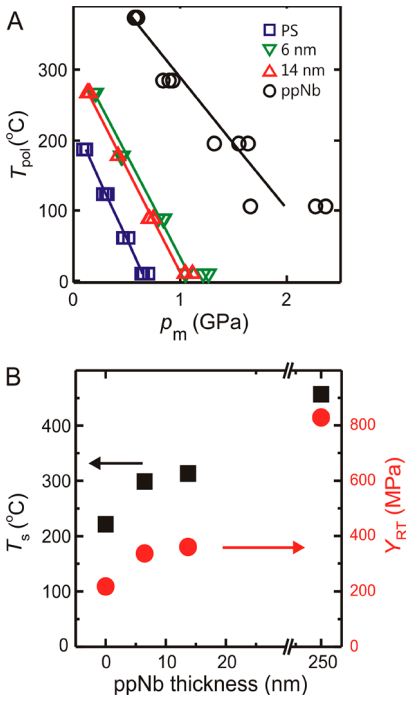

Figure 5. Analysis of the thermomechanical indentation data. (A) Master curves obtained from the indentation data according to eq 6. (B) Softening temperature T_s and yield stress Y plotted as a function of ppNb layer thickness.

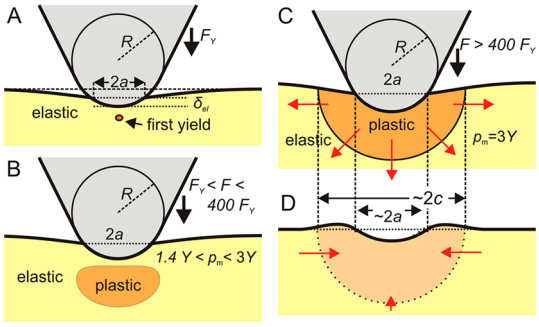

Figure 6. Indentation model according to Johnson.[26] (A) If $F < F_y$, the indentation is purely elastic and no permanent indent is formed. At $F = F_y$, first yield occurs below the indenter. (B) In the elastic-plastic regime, *i.e.*, at $F_y < F < 400\ F_y$, the plastically deformed volume is confined in an elastic matrix. (C) In the fully plastic regime, the plastically deformed volume has reached the surface. (D) After removal of the indenter, residual stresses are stored in the material, indicated by the red arrows. We assume that the inner radius of the indent is the same as the contact radius during indentation.

elasto-plastic regime. The material in the plastic volume reacts to the stress by permanent structural rearrangements similar to viscous flow. This in turn leads to a flattening of the local stress distribution, and simple elastic models cannot be applied. As a result, the elastic-plastic regime is difficult to capture in a simple model.

At even higher loads, the plastic volume reaches the surface of the polymer and is no longer contained within an elastic matrix (Figure 6C). In this so-called fully plastic regime, the stress distribution can be

approximated by a hemispherical sphere with radius a having a hydrostatic pressure component p_h. This inner "core" is enclosed in a hemispherical plastic volume (Figure 6C) of radius $c > a$. Outside the plastic volume, the deformations are elastic. For the simple model and elastic-perfect plastic solids, it has been found that the ratio between applied pressure p_m and yield stress Y only depends on the so-called nondimensional strain, which is a pure function of the indenter geometry.[26] In particular, in the fully plastic regime, the relation can be further reduced to

$$p_m \approx 3Y \quad (7)$$

Equation 7 rationalizes our corroboration of eq 5 and sets the scale. The values obtained for Y_{RT} can be seen on the right scale of Figure 5B. For PS the value is $Y_{PS} \approx$ 217 MPa.

Link to Macroscopic Experiments. PS is a model system in polymer physics. The glass transition temperature is $T_g \approx 100$ °C, and the tensile (compressive) yield stress is between 40 and 50 (70−90) MPa.[31] In our experiment, we measure significantly higher values of 220 °C for the softening temperature and 217 MPa for the yield strength. Our experiments are performed on length scales smaller than 10 nm and at indentation durations of less than 10 μs. We assign the effect predominantly to the very short interaction time of the hot tip with the sample surface in our experiment.

Above the glass transition, the time scale of structural relaxation is described by the WLF formalism and has been studied in detail for PS.[28,29] If we use the values cited in literature, we obtain a similar shift in the relaxation time scale by a temperature increase of approximately 38−43 °C above T_g, much less than the 120 °C shift observed here. On the other hand, we probe the polymer in the glassy regime and apply the temperature for durations much shorter than the structural relaxation time of the polymer. Therefore, glassy dynamics should describe the shift in time scale appropriately. Glassy dynamics are described by Arrhenius behavior, in the case of PS with an activation energy of 45−50 kcal/mol.[29] Assuming a typical time scale of the glass transition of 100 s, the observed shift in T_g of 120 °C corresponds to an activation energy of 49 kcal/mol, in perfect agreement with the literature values.

The yield stress is similarly subjected to a strong shift at short time scales. In our experiments, we achieve strain values on the order of $a/d \approx 0.5$ at a time scale of 10 μs, corresponding to a strain rate of $\approx 10^5$ s^{-1}. The yield stress measured in the experiment exceeds the yield stress measured at typical time scales of seconds by 130−180 MPa. The fast time scales are normally not accessible in traditional mechanical experiments. At normal rates, the yield strength is typically not strongly dependent on the time scale.[30] However, it has been observed that the yield strength increases rapidly on very fast time scales. For polycarbonate, an increase of ≈40 MPa per time decade has been observed at strain rates above 10^3 s^{-1}, which would be sufficient to explain the observed hardening.[30] In addition, we cannot exclude significant strain hardening due to the high strain values in our experiments.

Using the arguments above, the values obtained in the experiment can be rationalized. The two implicit conclusions are that we probe glassy dynamics at temperatures of more than 100 K above the glass transition temperature and that the yield stress increases significantly also for PS at very short time scales. Assuming the validity of the measured values, we can further analyze the elasto-plastic state of our indentations.

For this, we calculate the nondimensional strain of the indentations. The shape of our tips can be well described by a cone with a spherical apex at the end. The radius R of the sphere at the apex is about 5−10 nm, and the opening angle of the cone is 35 ± 5°. The nondimensional strain for a sphere is given by $E^*a/(YR)$. The effective elastic modulus E^* at room temperature and normal time scales is given by $E^* = E/(1 - \upsilon)^2 \approx 4$ GPa, where $E = 3.4$ GPa is the elastic modulus and $\upsilon = 0.38$ is the Poisson ratio for PS.[31] For our time scales, this value will increase slightly, we estimate by a factor of 1.5−2. This gives a lower limit for the nondimensional strain of ≈22 for the most shallow indents ($a = 6$ nm) and a 10 nm radius tip, which is still in the elasto-plastic regime but close to the border to the fully plastic regime of ≈40. For deeper written indents, the nondimensional strain increases until the cone of the indenter is reached. This gives an upper limit to the nondimensional strain at room temperature of $E^* \tan(90-35)/Y \approx 52$, which is in the fully plastic regime.

For the hot written indents, the elastic modulus is lower, but at the same time, the yield stress drops proportionally to the distance to the softening temperature, which is the dominating effect. Thus the nondimensional strain increases for the hot written indents, which puts these indents safely into the fully plastic regime. Therefore, most of our indentations were produced in the fully plastic regime, except for the shallow indents at room temperature, which are closer to the elasto-plastic regime. For these indents, we expect that more force is needed to produce a permanent indent of a certain depth. This is indeed observed in the data recorded at room temperature (see Figure 4F and Figure 5A; the data deviate from the straight line toward higher force values).

We would like to note that although we are in the so-called fully plastic regime, there is considerable elastic recovery during the indentation process. We can estimate the amount of elastic recovery assuming a perfectly elastic recovery using Hertzian contact mechanics.[26] In this model, the amount of elastic indentation for a spherical indenter is given by $\delta = (9F^2/(16RE^{*2}))^{1/3}$, and the mean pressure is given by

$p_m = \pi/4(6FE^{*2}/\pi^3R^2)^{1/3}$. Eliminating R, we obtain the elastic indentation for a given load and mean pressure: $\delta^2 = (9\pi/16)Fp_m/E^{*2}$. Neglecting the steeper pressure distribution of elastic indents, we may approximate the situation by the assumption that the elastic recovery of our fully plastic indentations is similar to the elastic penetration of a tip exerting a mean pressure p_m at a load F. If we use an effective elastic modulus of PS of $E^* = 1.5 \times E^*$ ($t = 1$ s) ≈ 6 GPa at 22 °C (see above) and the fast time scales, we arrive at elastic indentation depths of 1.5, 2.1, and 2.4 nm for the indents of 1.9, 3.6, and 5.4 nm permanent depth written at room temperature. Thus, we may estimate from the data that there may be up to 40% elastic recovery of the indentation for the shallowest indents at room temperature. This high amount of elastic recovery is also consistent with the linear $a(d_{rem})$ behavior shown in Figure 4G, which has been observed before to even smaller depth values.[19] The fact that we do not observe significant deviations for all samples indicates that the amount of elastic recovery is similar in all samples for a given indent depth.

For the ppNb-coated PS samples, we obtain a similar behavior as for the PS sample and the same analysis can be applied. The yield stress Y_{RT} at room temperature and the softening temperature T_s obtained from the master curve fit to the measured data are plotted in Figure 5B. As expected, the highly cross-linked bulk ppNb is a significantly harder and thermally more robust material than PS. The Y_{RT} value for ppNb is 4 times higher than for PS, 830 MPa *vs* 217 MPa, respectively, and the softening temperature of 457 °C is 2 times higher than the softening temperature of PS of 220 °C. For the layered materials with a 6 and 14 nm thick ppNb protective coating, we obtain effective softening temperatures of 299 and 314 °C, respectively, and RT yield stress values of 336 and 360 MPa, respectively.

An intriguing characteristic of the master curves is the fact that the slopes for the layered samples are indistinguishable from the slope of the master curve for the PS sample but markedly different from the slope of the master curve of the ppNb bulk sample. We take this as an indication that the plastic deformation in the layered samples is governed by yielding only in the PS sublayer. The top layer acts as an elastic skin, which screens part of the temperature and part of the pressure from the lower lying PS layer. This interpretation is supported by the fact that the bulk ppNb film has a much higher yield stress and softening temperature, which makes it unlikely that the thin layer of ppNb material would yield at the pressure and temperature levels used in embossing the indents into the layered samples.

One would further argue that the observed increase of the softening temperature of the layered samples at zero applied force is caused by thermal loss in the ppNb layer, whereas the measured increase of the Y_{RT} yield stress is a consequence of a reduction of the force acting on the PS layer due to the stiffness of the protective layer.

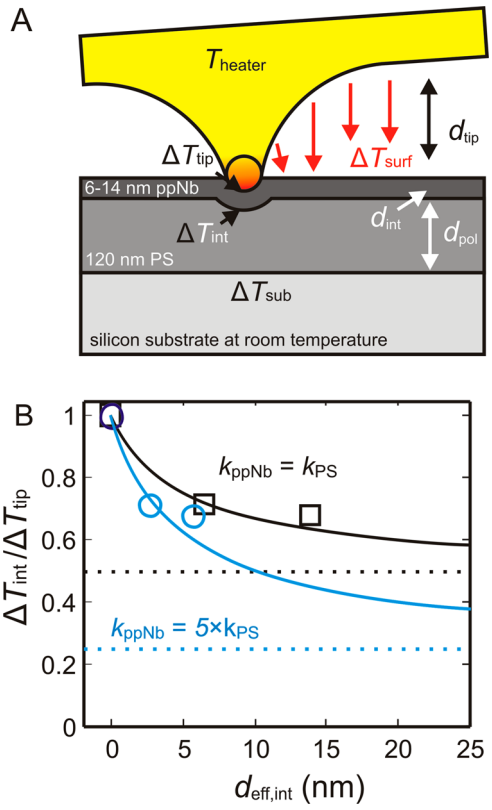

Figure 7. (A) Illustration of the thermal model used. A tip is heated by a heater at temperature T_{heater}. The heat sink is a silicon substrate which is considered to be at room temperature at its backside. (B) Measured relative values of the temperature drop at the interface $\Delta T_{int}/\Delta T_{tip}$ *vs* the interface thickness. Solid lines are calculated temperature profiles in the polymer assuming a ΔT_{surf} of 50 and 25% of the ΔT_{tip} (dotted lines).

Temperature Profiles in the Protection Layer. The measured softening temperature of the layered films is 78 and 93 K higher than T_s for the PS sample. Therefore, thermal shielding by the ppNb layer must be considered because plastic deformation for indent creation is located in the PS substrate (Figure 7A). The temperature distribution is determined by the tip heater as the heat source at elevated temperature (T_{heater}) and the silicon substrate acting as the heat sink at room temperature. Part of the generated heat is transferred through the tip into the sample. As argued above, the thermal resistance of the nanoscale tip is comparable to the thermal resistance of the polymer film; that is, the temperature at the tip−polymer interface T_{tip} is approximately half of the heater temperature with respect to room temperature. However, a second heat path exists through the air into the substrate as indicated by the red arrows in Figure 7A. The thermal conductivity of air (0.027 W m^{-1} K^{-1}) is approximately 5 times lower than the conductivity of PS (0.14 W m^{-1} K^{-1}).[32]

Therefore, a parallel plate heater at a distance of 500 nm above a 120 nm thick PS sample on a perfect heat sink (k_{Si} = 139 W m^{-1} K^{-1}) gives rise to a temperature increase of $d_{pol}/d_{tip} \times k_{air}/k_{PS}$, which amounts to 5% of the heater temperature. For heater temperatures of 450−600 °C, this approximately amounts to 20−30 K. In addition to the polymer heating, the silicon substrate may be heated locally (ΔT_{sub}). Haeberle *et al.* have determined the heating of a bare silicon substrate underneath a 440 °C hot heater to be 20 K.[33] Therefore, we may estimate an upper limit for the polymer surface heating of 50 K through air.

To determine the temperature increase caused by the hot tip in contact with the polymer surface, we assume in a first approximation of a homogeneous thermal sample that the thermal conductivity of PS (k_{PS}) and ppNb (k_{ppNb}) are the same. In this case, the temperature scales approximately with r^{-1} into the film.[34] Taking into account a 5 nm tip radius r_{tip} and the thicknesses d_{int} of 6.5 nm for the thinner and 13.7 nm for the thicker protection layer, we can calculate the expected increase in temperature at the interface ΔT_{int} using

$$\Delta T_{int} = \left(\frac{r_{tip}}{r_{tip} + d_{int}}\right) \Delta T_{pol} \qquad (8)$$

where ΔT_{pol} is the temperature rise of the polymer at the surface with respect to the polymer temperature ΔT_{surf} far from the tip contact ($\Delta T_{pol} = \Delta T_{tip} - \Delta T_{surf}$).

We found that the plastic deformation occurs in the PS material at the PS-ppNb interface. Therefore, we may estimate the temperature of the interface ΔT_{int} to be 220 °C at the softening transition. However, for the protected PS, we measured an increase in softening temperature to 299 and 314 °C, respectively (Figure 5B). The measured increase indicates that the temperature has dropped to 72 and 68% of the surface temperature ΔT_{tip} at the ppNb-PS interface ΔT_{int} using room temperature (25 °C) as reference. This ratio ($\Delta T_{int}/\Delta T_{tip}$) is plotted in Figure 7B *versus* the protection layer thickness (black squares). A good fit for eq 8 requires a polymer background temperature ΔT_{surf} of approximately 0.5 times the tip−polymer temperature ΔT_{tip} (black dotted line in Figure 7B), which amounts to 100−150 K. This is much higher than the estimated limit in temperature rise of 50 K calculated above.

Therefore, we have to take the different heat conductivities of the polymer layers k_{PS} and k_{ppNb} into account. A higher thermal conductivity of the ppNb layer leads to a proportionally reduced effective thickness for the heat transport. The thermal conductivity of PS, k_{PS} = 0.14 W m^{-1} K^{-1}, is low compared to other polymers in the amorphous glassy state, hence k_{ppNb} could be significantly higher (for example, polymethylmethacrylate has a thermal conductivity k_{PMMA} = 0.19 W m^{-1} K^{-1}). In addition, it is generally accepted that the thermal conductivity in a polymer is 10 times higher along the backbone of the chains than between different chains. Therefore, the highly cross-linked ppNb film should have a higher thermal conductivity value, and indeed, higher thermal conductivity of cross-linked polymers has been observed. Furthermore, the high compressive stresses in the tip−sample region may enhance the thermal conductivity further. Thus significantly higher thermal conductivity for ppNb is reasonable compared to PS. If we assume a 2.5 times higher thermal conductivity of the ppNb film, we can replace the interlayer thickness by a 2.5 times reduced thickness (Figure 7B, blue circles). In this case, the dotted blue line corresponds to a ΔT_{surf} of 0.25 times ΔT_{tip} corresponding to 50 K, in line with the estimated rise in surface temperature.

A similar argument can be put forward to explain the increase in yield strength of the samples with a protective ppNb layer. In a homogeneous film, the highest stress in an elastic indentation process occurs at a distance of ≈0.8a in the depth of the sample.[26] For the contact radii observed here, this amounts to a depth of 5−8 nm, similar to the thickness of the ppNb layers. In the layered systems, the stress distribution is more complex. Because strain is continuous at the interface, there is a discontinuity in the stress field at the interface, which leads to lower stress values in the softer PS layer. On the other hand, we measure a 4 times lower yield stress value for PS *versus* ppNb, which corroborates the interpretation that yield is nucleated in the PS layer. From the above arguments, it is clear that higher load values are needed to nucleate yield in the PS layer. Experimentally, we find that the overall yield stress of the layered systems is 1.5 and 1.7 times higher than that of the pure PS film, in line with our qualitative arguments.

CONCLUSION

In conclusion, we have studied the thermomechanical properties of protected PS films on the nanometer spatial and on the microsecond temporal scale using heatable scanning probes. We developed a unique indentation characterization method for polymers which relies on a small apex radius of the tips. Because of this property, nanoscale indentations in typical polymers occur in the fully plastic regime, which allows for a simple interpretation of the data. Using the model, we can characterize softening temperature and yield strength of polymers with and without protective coatings. We find softening temperatures of more than 100 K above T_g and yield stress values several times higher than those obtained by conventional methods. We attribute the effects to the short time scale of the force and, in particular, the temperature pulses. Remarkably, the high increase in softening temperature indicates that the polymers are probed in the glassy regime, although the applied temperatures are far

above the glass transition temperature. Because of the strong shift, the parameters obtained by the method cannot be compared directly to literature values. However, this new kind of microsecond nanoindentation opens up unique opportunities for studying polymer physics in a yet unexplored regime. It enables a sensitive screening of material parameters at a fast turnaround time. As demonstrated here, the method can clearly detect the mechanical differences caused by additional highly cross-linked ppNb protection layers as thin as 6.5 nm.

Using this method, we can characterize the differences of thermomechanical properties among the coated samples. We find that the protective coating acts as a thermal and mechanical barrier. It shields part of the temperature and stress from the PS sublayer, in which the plastic deformation is located. The increase of the softening temperatures can be explained by macroscopic heat transport equations. Our analysis indicates that the protective coating has a significantly higher thermal conductivity than the PS film.

For data storage applications, the PS/norbornene system is a significant step forward from previous materials. We have achieved a physical separation of the material which is plastically yielding and the material in contact with the tip on the nanometer scale. The coating protects the tip and the sample from deformations induced by the shear forces involved in scanning the tip to read out the data. The retention of the data is given by the stability of the plastic deformation in the sublayer. The sublayer can be tuned to find the optimal trade-off between softness and retention capabilities. Low-power operation and increased tip lifetimes can be expected from the lower tip−sample forces and temperatures involved in writing. As a general scheme, the protective coating allows the use of un-cross-linked storage media, which enriches the choice of materials and the ease of implementation.

METHODS

Sample Preparation. Bilayer films were deposited on N-doped (0.01/cm) silicon [100] wafers (Siltronic AG). After cutting the wafers into pieces of 2.5 × 2.5 cm^2, they were rinsed with Milli-Q water and ethanol to remove residues. Then the wafers were dried using an air gun. To avoid contamination, the wafer pieces were stored in glass vessels after cleaning. The PS (molecular weight M_w of 100.000 g/mol) films were prepared by spin coating from a 2 wt % solution of polystyrene in toluene. The spin coater was ramped up to 2000 rpm at an acceleration of 5000 rpm/s^2 and was operated for 100 s. The PS film thickness ranges from 100 to 120 nm as determined from profilometry and X-ray reflectivity (XRR) measurements. Films of cross-linked norbornene were deposited on Si and PS covered Si wafers using a cylindrical (100 mm Ø, 300 mm long 13.56 MHz) pyrex plasma reactor.[35] For the plasma polymerization process of norbornene (Sigma-Aldrich, 99% purity, bp 65 °C, vapor pressure 52 mbar at 25 °C), a pressure of 0.05 mbar was adjusted in the reactor using needle valves at the norbornene storage vessel and throttle valves at the vacuum pump. The radio frequency (RF) source (Coaxial Power Systems Ltd., Eastbourne) was connected to the reactor coil antenna *via* a matching system. Details of the used reactor are described elsewhere.[35] For the deposition of wear-resistive plasma-polymerized norbornene (ppNb) films, we used a plasma input power of 150 W. The thickness of the norbornene protection layers was adjusted by the time the plasma reactor is switched on. In the case of a PS surface, we calculated a deposition rate of ≈10 nm/s. Thus for the deposition of hyper-thin films in the order of 10 nm, we used a plasma deposition time of ≈1 s.

The thickness of the single-layer and bilayer layer films was measured using a profilometer (KLA-Tencor P-16+, Milpitas, USA) across scratches made by a sharp needle. The films thicknesses were calculated as the mean value of the height difference between scratch and film surface at six different positions. The standard deviation in the measurement of the thickness can reach 5 nm. Therefore, the thickness of hyper-thin films (<10 nm) could not be reliably measured in this way. Thus, X-ray reflectivity (XRR) measurements were performed for determining the thickness of the layers in the bilayer film. For this purpose, 1 × 1 cm^2 samples were analyzed in a Seifert XTD 3003 TT X-ray diffraction system (Seifert, Ahrensburg, Germany). The diffractometer was operated in reflectivity mode with a multilayer mirror as a monochromator at a fixed wavelength of $\lambda = 1.54$ Å. The beam size was 1000 × 100 μm^2 (horizontal × vertical) having a resolution in $q_z = 6 \times 10^{-3} \pm 2 \times 10^{-3}$ $Å^{-1}$. A formalism based on Parrat's work was used for fitting a model to the reflectivity data which allowed us to determine the exact thickness of the thick PS sublayer and the hyper-thin plasma-polymerized norbonene (ppNb) layer with 0.1 nm precision.[15] Surface roughness and wear resistivity[16] were assessed using scanning force microscopy (NanoWizard, JPK, Berlin, Germany; Veeco D3100, Santa Barbara, CA, USA) using cantilever probes with a nominal spring constant of 0.2 N/m (Cont-W, NanoWorld, Neuchatel, Switzerland), and the spring constant was calibrated by the thermal tune method.[36] Surface wear tests were performed at a normal force of 10 nN. An area of 3 μm × 3 μm was scanned 100 times at a velocity of 50 μm/s. Afterward, the wear-tested areas were imaged at a scan size of 5 μm × 5 μm. We quantified the mechanical stability of the film by analyzing the root-mean-square roughness on an area of 1 μm × 1 μm inside the wear-tested area.

Contact angle measurements (OCA35, DataPhysics Instruments Gmbh, Filderstadt, Germany) were used to probe the hydrophilicity of a surface. The samples were probed using Milli-Q water.

Thermomechanical Writing and Temperature Calibration. The indentation experiments were performed on a home-built test station under controlled low humidity, <1%, nitrogen atmosphere. The silicon indenter tip with a height of 500−700 nm and an apex radius of ≈5 nm is placed on top of a low-doped resistive heater element of the cantilever sensor. The sensor also comprises a capacitive platform for applying load forces by electrostatic means and a resistive read sensor made of low-doped Si for thermoelectrically measuring the relative motion of the tip with respect to the sample. A capacitive platform in the center provides a large capacitance to the sample and therefore an effective actuation mechanism to pull the tip into contact and to control the applied force.

For writing, the tip is approached by mechanical means to its rest position at a distance of ≈50−300 nm above the surface. The tip heater is heated to the writing temperature using a constant voltage excitation. For a write operation, the tip is pulled into contact by applying an electric potential between the conducting Si substrate and the capacitive platform of the silicon cantilever.

Temperature calibration of the heater is done by measuring a current−voltage (*IV*) response curve of the heater. The resistance of the heater is plotted as a function of dissipated power. The temperature at which the maximum resistance occurs is a function of the silicon doping density and is known as inversion

temperature. We assume that all of the power dissipated in the cantilever contributes to the heating of the heater structure and that the temperature change of the heater is a linear function of the dissipated power. For the doping values used here, the maximum resistance occurs at 550 °C.

The temperature reached in the polymer during a write operation is a complex function of the tip geometry and depends on the heat resistance of the tip, the resistance of the interface between tip and polymer, and the polymer's heat-spreading resistance, including the underlying substrate in the case of a thin polymer film (≤100 nm). In particular, it depends on the contact radius and the opening angle of the tip (20−50° for our tips). In the text, we cite the heater temperatures only. A rough estimation states that the increase in polymer temperature is approximately half the tip heater temperature relative to room temperature.[20,21]

Thermomechanical Reading. The read resistor of the cantilever sensor is heated to ≈200 °C using a constant voltage excitation. The temperature of the heater depends on the width of the air gap between the heater and the sample, which acts as a cooling path. The temperature, in turn, determines the heater resistance which is measured *via* the heater current using a virtual ground current to voltage converter. Thus the heater current of the Si heater is a direct measure of the vertical distance of the cantilever structure to a coarse-grained average sample plane. The thermal time constant of the reader is ≈5 μs, and the overall noise level corresponds to a 0.1 nm_{rms} resolution of the tip−sample distance measurement.

For topography imaging, an effective load force of ≤10 nN is applied. In addition, high-frequency force modulation is used to excite resonant modes in the MHz range of the cantilever. The high-order mode acts as a stiff system for modulating the tip−sample distance, and a vibration amplitude of 1 nm is sufficient to overcome the adhesion interaction. The soft cantilever provides a force-controlled support for the vibrating tip, enabling high-speed intermittent contact force microscopy without feedback control of the cantilever bending.

Conflict of Interest: The authors declare no competing financial interest.

Acknowledgment. We thank B. Gotsmann and M. Robbins for stimulating discussions. The microcantilevers used in the experiments were fabricated by U. Drechsler, R. Stutz, and Michel Despont from the microfabrication group at the IBM Research—Zurich Laboratory. We acknowledge the support from the Deutsche Forschungsgemeinschaft (DFG) within the Strategic Japanese German Cooperative Programme on Nanoelectronics (BE3286/2-1; GU 771/6-1), and SPP1369 Priority Program (Polymer−Solid Contacts: Interfaces and Interphases) for partial funding. This work was supported by the European Research Council under the project ProTem. Y.Z. thanks the Alexander von Humboldt foundation for financial support.

REFERENCES AND NOTES

1. Eleftheriou, E.; Antonakopoulos, T.; Binnig, G.; Cherubini, G.; Despont, M.; Dholakia, A.; Durig, U.; Lantz, M.; Pozidis, H.; Rothuizen, H.; *et al.* Millipede—A MEMS-Based Scanning-Probe Data-Storage System. *IEEE Trans. Nanotechnol.* **2003**, *39*, 938–945.
2. Gotsmann, B.; Knoll, A. W.; Pratt, R.; Frommer, J.; Hedrick, J. L.; Duerig, U. Designing Polymers To Enable Nanoscale Thermomechanical Data Storage. *Adv. Funct. Mater.* **2010**, *20*, 1276–1284.
3. Hiller, J.; Mendelsohn, J.; Rubner, M. Reversibly Erasable Nanoporous Anti-reflection Coatings from Polyelectrolyte Multilayers. *Nat. Mater.* **2002**, *1*, 59–63.
4. Lin, Y.; Yasuda, H. Effect of Plasma Polymer Deposition Methods on Copper Corrosion Protection. *J. Appl. Polym. Sci.* **1996**, *60*, 543–555.
5. Yamamoto, T.; Okubo, M.; Imai, N.; Mori, Y. Improvement on Hydrophilic and Hydrophobic Properties of Glass Surface Treated by Nonthermal Plasma Induced by Silent Corona Discharge. *Plasma Chem. Plasma Process.* **2004**, *24*, 1–12.
6. Klages, C. P.; Dietz, A.; Höing, T.; Thyen, R.; Weber, A.; Willich, P. Deposition and Properties of Carbon-Based Amorphous Protective Coatings. *Surf. Coat. Technol.* **1996**, *80*, 121–128.
7. Chifen, A. N.; Jenkins, A. T. A.; Knoll, W.; Forch, R. Adhesion Improvement of Plasma-Polymerized Maleic Anhydride Films on Gold Using HMDSO/O2 Adhesion Layers. *Plasma Processes Polym.* **2007**, *4*, 815–822.
8. Zajíčková, L.; Bursíková, V.; Kučerová, Z.; Franta, D.; Dvorák, P.; Smíd, R.; Perina, V.; Macková, A. Deposition of Protective Coatings in Rf Organosilicon Discharges. *Plasma Sources Sci. Technol.* **2007**, *16*, S123.
9. Yasuda, H. Glow Discharge Polymerization. *J. Polym. Sci.: Macromol. Rev.* **1981**, *16*, 199–293.
10. Bhushan, B.; Li, X. Nanomechanical Characterisation of Solid Surfaces and Thin Films. *Int. Mater. Rev.* **2003**, *48*, 125–164.
11. Sirghi, L.; Ruiz, A.; Colpo, P.; Rossi, F. Atomic Force Microscopy Indentation of Fluorocarbon Thin Films Fabricated by Plasma Enhanced Chemical Deposition at Low Radio Frequency Power. *Thin Solid Films* **2009**, *517*, 3310–3314.
12. Pollock, H.; Hammiche, A. Micro-Thermal Analysis: Techniques and Applications. *J. Phys. D: Appl. Phys.* **2001**, *34*, R23–R53.
13. McConney, M.; Singamaneni, S.; Tsukruk, V. Probing Soft Matter with the Atomic Force Microscopies: Imaging and Force Spectroscopy. *Polym. Rev.* **2010**, *50*, 235–286.
14. Nelson, B.; King, W. Measuring Material Softening with Nanoscale Spatial Resolution Using Heated Silicon Probes. *Rev. Sci. Instrum.* **2007**, *78*, 023702–023702.
15. Parratt, L. G. Surface Studies of Solids by Total Reflection of X-rays. *Phys. Rev.* **1954**, *95*, 359.
16. Berger, R.; Cheng, Y.; Förch, R.; Gotsmann, B.; Gutmann, J. S.; Pakula, T.; Rietzler, U.; Schärtl, W.; Schmidt, M.; Strack, A.; *et al.* Nanowear on Polymer Films of Different Architecture. *Langmuir* **2007**, *23*, 3150–3156.
17. Leung, O. M.; Goh, M. C. Orientational Ordering of Polymers by Atomic Force Microscope Tip−Surface Interaction. *Science* **1992**, *255*, 64–66.
18. Pantazi, A.; Sebastian, A.; Antonakopoulos, T. A.; Bächtold, P.; Bonaccio, A. R.; Bonan, J.; Cherubini, G.; Despont, M.; DiPietro, R. A.; Drechsler, U.; *et al.* Probe-Based Ultrahigh-Density Storage Technology. *IBM J. Res. Dev.* **2008**, *52*, 493–511.
19. Altebaeumer, T.; Gotsmann, B.; Pozidis, H.; Knoll, A.; Duerig, U. Nanoscale Shape-Memory Function in Highly Cross-Linked Polymers. *Nano Lett.* **2008**, *8*, 4398–4403.
20. Gotsmann, B.; Lantz, M. A.; Knoll, A.; Duerig, A. Nanoprobes. In *Nanotechnology*; Fuchs, H., Ed.; VCH: Weinheim, Germany, 2009; Vol. 6, pp 121−169.
21. The contact radius increases for deeper indents, which may affect the polymer temperature. There are several competing effects which influence the polymer surface temperature as a function of contact area. In general, the temperature distribution can be approximated by considering the various thermal resistances between the heater and the silicon substrate, *e.g.*, the tip resistance, the interfacial resistance, and the thermal spreading resistance in the polymer. While the interfacial resistance decreases linearly with contact area, the spreading resistance decreases with the linear contact dimension. As a result, the effects partially compensate each other. Experimentally, we do not observe variations in the softening temperature with indent depth; see Figure 4F. If the temperature would significantly change for deeper indents, the extrapolation for these indents would yield a different softening temperature.
22. Robertson, R. E. Theory for the Plasticity of Glassy Polymers. *J. Chem. Phys.* **1966**, *44*, 3950–3956.
23. Bauwens-Crowet, C.; Bauwens, J.; Homès, G. The Temperature Dependence of Yield of Polycarbonate in Uniaxial Compression and Tensile Tests. *J. Mater. Sci.* **1972**, *7*, 176–183.
24. Rottler, J.; Robbins, M. O. Shear Yielding of Amorphous Glassy Solids: Effect of Temperature and Strain Rate. *Phys. Rev. E* **2003**, *68*, 011507.

25. Altebaeumer, T.; Gotsmann, B.; Knoll, A.; Cherubini, G.; Duerig, U. Self-Similarity and Finite-Size Effects in Nano-Indentation of Highly Cross-Linked Polymers. *Nanotechnology* **2008**, *19*, 475301.
26. Johnson, K. L. *Contact Mechanics*.; Cambridge University Press: Cambridge, 1994; p XI, 452 S.
27. F is the effective force on the tip. This force is given by the applied load F_{app} reduced by the restoring force of the tip at a given indent depth d_{ind}: $F = F_{app} - k_{tip}d_{ind}$, where k_{tip} is the spring constant of the cantilever used. The restoring spring force is in the order of 5 nN ($k_{tip} \approx 1$ N/m). We approximate by assuming $d_{ind} \approx d_{rem}$.
28. Pschorn, U.; Rössler, E.; Sillescu, H.; Kaufmann, S.; Schaefer, D.; Spiess, H. Local and Cooperative Motions at the Glass Transition of Polystyrene: Information from One- and Two-Dimensional NMR as Compared with Other Techniques. *Macromolecules* **1991**, *24*, 398–402.
29. Dhinojwala, A.; Wong, G. K.; Torkelson, J. M. Rotational Reorientation Dynamics of Disperse Red 1 in Polystyrene: Alpha-Relaxation Dynamics Probed by Second Harmonic Generation and Dielectric Relaxation. *J. Chem. Phys.* **1994**, *100*, 6046–6054.
30. Richeton, J.; Ahzi, S.; Daridon, L.; Rémond, Y. A Formulation of the Cooperative Model for the Yield Stress of Amorphous Polymers for a Wide Range of Strain Rates and Temperatures. *Polymer* **2005**, *46*, 6035–6043.
31. Van Krevelen, D. *Properties of Polymers: Their Correlation with Chemical Structure; Their Numerical Estimation and Prediction from Additive Group Contributions*; Elsevier B.V.: Amsterdam, 1997.
32. Brandrup, J.; Immergut, E.; Grulke, E.; Abe, A.; Bloch, D. *Polymer Handbook*; Wiley: New York, 1999.
33. Haeberle, W.; Pantea, M.; Hoerber, J. K. H. Nanometer-Scale Heat-Conductivity Measurements on Biological Samples. *Ultramicroscopy* **2006**, *106*, 678–686.
34. Duvigneau, J.; Schönherr, H.; Vancso, G. J. Nanoscale Thermal AFM of Polymers: Transient Heat Flow Effects. *ACS Nano* **2010**, *4*, 6932–6940.
35. Chu, L. Q.; Knoll, W.; Förch, R. Stabilization of Plasma-Polymerized Allylamine Films by Ethanol Extraction. *Langmuir* **2006**, *22*, 5548–5551.
36. Hutter, J. L.; Bechhoefer, J. Calibration of Atomic-Force Microscope Tips. *Rev. Sci. Instrum.* **1993**, *64*, 1868–1873.